JOURNAL OF GEOPHYSICAL RESEARCH, VOL. 100, NO. D10, PAGES 20,999–21,012, OCTOBER 20, 1995

Dry deposition parameterization in a chemistry general circulation model and its influence on the distribution of reactive trace gases

Laurens Ganzeveld and Jos Lelieveld

Department of Air Quality, Wageningen University, Wageningen, Netherlands

Abstract. A dry deposition scheme has been developed for the chemistry general circulation model to improve the description of the removal of chemically reactive trace gases at the earth's surface. The chemistry scheme simulates background CH_4-CO-NO_x-HO_x photochemistry and calculates concentrations of, for example, HNO_3, NO_x, and O_3. A resistance analog is used to parameterize the dry deposition velocity for these gases. The aerodynamic resistance is calculated from the model boundary layer stability, wind speed, and surface roughness, and a quasi-laminar boundary layer resistance is incorporated. The stomatal resistance is explicitly calculated and combined with representative cuticle and mesophyll resistances for each trace gas. The new scheme contributes to internal consistency in the model, in particular with respect to diurnal and seasonal cycles in both the chemistry and the planetary boundary layer processes and surface characteristics that control dry deposition. Evaluation of the model indicates satisfactory agreement between calculated and observed deposition velocities. Comparison of the results with model simulations in which the deposition velocity was kept constant indicates significant relative differences in deposition fluxes and surface layer trace gas concentrations up to about ±35%. Shortcomings are discussed, for example, violation of the constant flux approach for the surface layer, the lacking canopy description, and effects of surface water layers.

1. Introduction

The removal of gases and particles from the atmosphere by turbulent transfer and uptake at the Earth's surface is a primary mechanism to cleanse the atmosphere and deliver chemical doses to the surface [*Wesely*, 1989]. This removal of trace gases at the surface by chemical, physical, and biological processes, in the absence of precipitation, is defined as dry deposition. The dry deposition flux of trace gases is often parameterized in models as the concentration of the trace gas at a specific height multiplied by a deposition velocity (V_d), which depends on atmospheric parameters as well as specific surface parameters. This deposition velocity is usually expressed in terms of an aerodynamic resistance, which is a function of the physical state of the atmosphere and a surface resistance, which is a function of the chemical, physical and biological properties of the surface [*Chameides*, 1987]. Measurement campaigns have confirmed the dependence of the deposition velocity on surface characteristics [*Fuentes et al.*, 1992; *Lenschow et al.*, 1982; *Baldocchi*, 1993; *Massman et al.*, 1994]. Uptake by the vegetation is a major sink for many trace gases and deposition velocities are related to the diurnal and seasonal cycles in plant activity and specific physical properties of the vegetation. Also, for surfaces covered by water layers or sparse vegetation the uptake processes can show a temporal dependence and relations with site specific physical properties, for example, the presence of snow or ice.

A dry deposition model, similar to that presented by *Hicks et al.* [1987], has been incorporated in the European Centre Hamburg Model (ECHAM) which has been coupled to a chemistry scheme [*Roelofs and Lelieveld*, 1995] to improve the description of the removal of chemically reactive trace gases. Different descriptions of the dry deposition process on a global scale have been used in previous studies. *Penner et al.* [1991] use a constant deposition velocity for each trace gas, while *Dentener and Crutzen* [1993], *Levy and Moxim* [1989], and *Kasibhatla et al.* [1993] use a constant surface uptake rate, derived from observed deposition velocities, and a parameterization of turbulent transfer calculated from the drag coefficient. An inventory of the global distribution of emission and dry deposition velocities of trace gases by *Müller* [1992] takes into account a surface uptake rate dependent on surface characteristics. However, *Müller* [1992] calculates deposition velocities from assumed surface uptake rates and constant turbulent transport rates. Our scheme calculates deposition velocities according to the "big-leaf" concept [*Hicks et al.*, 1987] from the turbulent transfer and vegetation activity computed by the ECHAM model, supplemented with representative uptake rates for soil, water, and snow/ice on a global scale. The main purpose of the development of this more comprehensive dry deposition scheme for ECHAM is to improve the description of trace gas exchange between the atmosphere and the surface, consistent with temporal and spatial dependencies of the model physics and chemistry. Moreover, the degree of detail of the new dry deposition parameterization should be compatible with that of other process descriptions in ECHAM. We emphasize that the scheme uses all the relevant ECHAM calculated parameters. It is not expected that it reproduces local observed deposition velocities since differences between the spatial and temporal scales of ECHAM and micrometeorological processes may be

Paper number 95JD02266.
0148-0227/95/95JD-02266$05.00

large. However, the scheme should catch the specific global scale differences between distinct receptor surfaces exposed to very different meteorological conditions, for example, equatorial tropical forest, desert, high-latitude tundra, etc. We will show that the scheme succeeds in simulating deposition velocities which are in reasonable agreement with observations although further improvements must be incorporated in future model versions.

2. The ECHAM Model

The GCM used in this study is the ECHAM model (version 3.2) which evolved from the numerical weather prediction model developed at the European Centre for Medium Range Weather Forecasts (ECMWF) [*Roeckner et al.*, 1992]. We use a T21 horizontal resolution corresponding with grids squares of about 5.6 deg and a time step of 40 min. The model has 19 vertical layers in a hybrid σ-p coordinate system. Prognostic variables are vorticity, divergence, temperature, surface pressure, humidity, and cloud water. The model contains parameterizations of radiation, cloud formation and precipitation, convection and horizontal and vertical diffusion. The seasonal cycle of the sea surface temperature is prescribed as a boundary condition. Land surface processes are described by a five-layer heat conductivity soil model and by a hydrological model to determine evaporation and runoff [*Lohmann et al.*, 1993]. Over land, each grid square is subdivided into four fractions to distinguish between snow coverage, bare soil, water in the skin reservoir (water stored within the canopy and on bare soil) and vegetation. Permanent ice cover over land is prescribed by a glacier mask. The vegetation fraction of each grid square is representative for the biological state of the vegetation type assigned to each grid square according to *Wilson and Henderson-Sellers* [1985]. Their classification system discerns 6 major ecotype classes. Over land the roughness length is geographically prescribed while over ice-free sea it is calculated following *Charnock* [1955] [*Deutsches Klimarechenzentrum, Modellbetreuungsgruppe (DKRZ)*, 1992, and references therein]. Transport of water vapour and trace gases is described by a semi-Lagrangian advection scheme. The ECHAM model is coupled to a chemistry scheme developed by *Roelofs and Lelieveld* [1995]. The scheme calculates the NO_y (NO/NO_2, HNO_3, HNO_4, NO_3, and N_2O_5), OH and O_3 concentrations based on the background CH_4-CO-NO_x-HO_x photochemistry taking into account the role of nighttime chemical reactions of HNO_3 and N_2O_5 on aerosol surfaces and clouds, and the resulting loss of NO_x [*Dentener and Crutzen*, 1993]. Emissions of NO_x, CO, and CH_4 are considered and the wet deposition calculations use the ECHAM parameterization schemes for large-scale and convective clouds [*Roelofs and Lelieveld*, 1995].

3. Dry Deposition Parameterization

3.1. Theory

The concentration of a trace gas [c] in the atmosphere, adjacent to the Earth's surface, is determined by transport, chemical production or destruction, emission, and wet and dry deposition:

$$\frac{dc}{dt} = \left(\frac{\partial c}{\partial t}\right)_{\text{transp}} + \left(\frac{\partial c}{\partial t}\right)_{\text{chem}} + \left(\frac{\partial c}{\partial t}\right)_{\text{emiss}} + \left(\frac{\partial c}{\partial t}\right)_{\text{dep}} \quad (1)$$

The contribution of dry deposition is explicitly expressed by a relationship between the deposition flux and deposition velocity according to

$$F_c = c_z V_d \quad (2)$$

where F_c is the deposition flux of the trace gas (molecules m^{-2} s^{-1}), c_z is the concentration of the trace gas (molecules m^{-3}) at a reference height z, and V_d is the deposition velocity (m s^{-1}) at the reference height z. The time integrated dry deposition flux is hereafter referred to as "deposition." The deposition velocity is assumed to be independent of the concentration of the trace gas of interest and to be related to specific characteristics of surfaces and the atmospheric conditions above these surfaces:

$$V_d = \frac{1}{R_a + R_b + R_{\text{surf}}} \quad (3)$$

where R_a is the aerodynamic resistance, which is a function of the turbulence in the surface layer, R_b is the quasi-laminar boundary layer resistance (QBR), partially controlled by molecular diffusion, and R_{surf} is the combined resistance of all transfer pathways which play a role in the uptake of trace gases by the surface.

3.2. Aerodynamic- and Quasi-laminar Boundary Layer Resistance

The aerodynamic resistance is given by

$$R_a = \frac{1}{u_* k}\left[\ln\left(\frac{z-d}{z_0}\right) - \Psi\left(\frac{z-d}{L}\right)\right] \quad (4)$$

where u_* is the friction velocity (m s^{-1}), k is the Von Karman's constant ($\approx$0.4), z is the reference height which is half the average height of the model's lowest layer (about 60 m, so $z \approx$ 30 m) and Ψ is a dimensionless stability correction term which is a function of the height and a height independent stability parameter L (meters) (Monin-Obukhov length); d is the displacement height (meters), which is introduced in the calculation of R_a over surfaces with relatively large obstacles (often taken as 2/3 of the canopy height). However, in our scheme the displacement height is assumed to be zero since d is already incorporated in the model's surface level. For the roughness length, z_0, a characteristic length scale of the underlying surface, the surface roughness for momentum z_{0m} as used in the ECHAM model [*DKRZ*, 1992] is used. The stability correction term is calculated from the model's stability in the lowest model layer based on the *Dyer and Hicks* [1970] flux profile relationships for heat [*Brutsaert*, 1973, and references therein].

The aerodynamic resistance for a specific trace gas X (R_{aX}) can be expressed as the sum of the aerodynamic resistance, and an additional quasi-laminar boundary layer resistance R_{bX}. This resistance arises in the trace gas flux calculations because of different roughness lengths for momentum (z_{0m}) and trace gases (z_{0X}) [*Fuentes et al.*, 1992, and references therein]:

$$R_{aX} = R_a + \ln\left(\frac{z_{0m}}{z_{0X}}\right)\frac{1}{k u_*}(Sc/Pr)^{2/3} \quad (5)$$

where the second term on the right-hand side represents R_{bX}, Sc is the Schmidt number defined as the ratio of the kinematic viscosity for air (0.15 cm^2 s^{-1}) and the molecular diffusivity of the trace gas (at 1013.25 mbar) and Pr is the Prandtl number (0.72) [*Hicks et al.*, 1987]. For vegetated areas a value of 2 has been adopted for $\ln(z_{0m}/z_{0X})$ [*Garrat and Hicks*, 1973]. For snow, ice, water, and bare soil the surface roughness for momentum (z_{0m}) ranges from about 0.001 up to 0.1 cm. According to *Brutsaert* [1973] for this range the surface roughness for

trace gases is about 3 times smaller than for momentum, yielding a logarithmic ratio ln (z_{0m}/z_{0X}) of about 1. Since R_{bX} is often significantly smaller than R_a and R_{surf}, the computation of the deposition velocity for a specific trace gas, V_{dX}, will not be very sensitive to the chosen definition of R_{bX}. This will also be shown in the presentation of the results (section 4).

3.3. Surface Resistance

In the ECHAM model, each land grid square is divided into four subgrids, defined by a snow (ice) covered fraction, one with water in the skin reservoir, one with bare soil and one with vegetation [*DKRZ*, 1992], while over sea the seaice covered fraction is defined. The surface resistance of compound X of the sea and wet skin reservoir, snow, ice, and bare soil is defined by

$$R_{surf} = r_{wat/snow/ice/soil} \tag{6}$$

and that over vegetation by

$$R_{surf} = \frac{1}{LAI/r_{leaf} + 1/r_{soil}} \tag{7}$$

where LAI is the single-side total area of leaves/needles per area surface, r_{leaf} is the leaf/needle resistance which is the resultant resistance of the serial mesophyll and stomatal resistance, r_{mes} and r_{stom}, and a parallel cuticular resistance, r_{cut}. The relative importance of r_{soil} in (7) increases with a decreasing LAI; locations without vegetation have an LAI of zero. In ECHAM the r_{stom} of the canopy is calculated as a function of the photosynthetically active radiation (PAR) and the available water in the root zone $F(W_s)$ according to *Sellers et al.* [1986]:

$$r_{stom} = \frac{kc}{\left[\frac{b}{d\mathrm{PAR}} \ln\left(\frac{de^{kLAI}+1}{d+1}\right) - \ln\left(\frac{d+e^{-kLAI}}{d+1}\right)\right] F(W_s)} \tag{8}$$

where $d = (a + b^*c)/(c^*\mathrm{PAR})$, $k = 0.9$, $a = 5000$ J m^{-3}, $b = 10$ W m^{-2}, and $c = 100$ s m^{-1}. Equation (8) is used to determine the r_{stom} for the trace gas of interest for a leaf/needle of any vegetation type, using an LAI of 1, and corrected for differences in molecular diffusivity between H_2O and the trace gas and then combined with r_{cut} and r_{mes} yielding r_{leaf}. The state of the canopy in this ECHAM version is not expressed by the LAI, which has a constant value of 4 for all vegetation types, independent of time and location, but by a seasonally dependent vegetation area fraction, representative for each of the six vegetation classes assigned to each grid square according to *Wilson and Henderson-Sellers* [1985]. This vegetation area fraction accounts for both the amount of standing biomass and the capacity for uptake of trace gases of the vegetation type in each grid square. The grid-average deposition velocity is computed as the area weighted average of the deposition velocities for each subgrid fraction from R_{aX} and the R_{surf}.

The current dry deposition parameterization in ECHAM is developed for the trace gases O_3, HNO_3, and NO_x (NO and NO_2). Ozone plays a key role in the chemistry of the troposphere and its destruction at the underlying surfaces needs to be realistically represented [*Galbally et al.*, 1980]. Uptake processes of ozone at the surface, especially by vegetation, are relatively straightforward to compute compared to other trace gases, like SO_2 and NO_x. For the latter trace gases R_{surf} is codetermined by a number of complex processes, for example, uptake of SO_2 and reactions within water layers on the vegetation (dew, rain) and soil emissions (NO_x). Measurements in different vegetated locations have shown that the dry deposition of O_3 is controlled by r_{stom} and R_{aX} since r_{cut} is relatively large [*Kerstiens and Lendzian*, 1989] and $r_{mes} \approx 0$ [*Wesely*, 1989; *Neubert et al.*, 1993]. The uptake by soil and water surfaces, however, is still uncertain. NO_x is of major importance for the photochemical production of O_3, and HNO_3 serves as a reservoir species for NO_x in remote locations, releasing it through photolysis and reaction with the OH radical. Deposition parameterization of additional species, for example, SO_2, H_2O_2, NO_3, N_2O_5, CH_3O_2H, and aerosol particles, will be incorporated in future versions of the scheme. The concentrations of short-lived trace gases like HO_2, OH, CH_3O_2, and CH_2O are largely determined by chemical reactions and not by dry deposition. In the next section, representative resistances of all uptake pathways are presented for O_3, HNO_3, NO and NO_2.

3.3.1. Ozone

In this section we distinguish ozone uptake resistances for vegetation, soil, water, snow, and ice.

Vegetation: It is generally assumed that the internal leaf concentration of O_3 equals zero, which leads to a zero O_3 mesophyll resistance. The uptake of O_3 by the cuticle is small compared to the uptake through the stomata [*Kerstiens and Lendzian*, 1989], which means that this transfer pathway can be neglected in the parameterization of r_{leaf} [*Baldocchi et al.*, 1987]. Thus uptake of O_3 by vegetation is solely determined by the stomatal resistance. A large cuticle resistance for O_3 of 10^5 s m^{-1} has been adopted.

Soil: Measurements of O_3 uptake by soils show a soil type dependence as well temporal variations in the soil resistance, with typical values ranging from about 50 up to 1000 s m^{-1} [*Galbally and Roy*, 1980; *Stocker*, 1993; *Wesely*, 1981, 1989]. Temporal variations in r_{soil} can be due to variations in soil wetness and temperature. In many experiments a strong dependency of the r_{soil} for O_3 on the soil water content was found [*Galbally and Roy*, 1980, and references therein; *Wesely*, 1981; *Van Pul*, 1992]. In the current version of the model a constant value of r_{soil} of 400 s m^{-1} is used, which is larger than that of *Wesely* [1989], *Leuning et al.* [1979], *Van Pul* [1992], and *Galbally and Roy* [1980]. However, most of these values were measured under summer conditions. *Wesely* [1981] observed a considerably higher r_{soil} of about 1000 s m^{-1} for cold bare soil, which is consistent with an observed ozone deposition velocity of about 0.10 cm s^{-1} above a deciduous forest floor [*Hicks et al.*, 1989, and references therein]. *Stocker et al.* [1993] measured O_3 fluxes over a shortgrass prairie from March to August and derived an average r_{soil} of about 400 s m^{-1}. This value of 400 s m^{-1} is assumed to be representative throughout the year for all soil types.

Water, snow, and ice: The deposition of O_3 on water surfaces is small compared to deposition to land surfaces. Measured deposition velocities are of the order of 0.01 cm s^{-1} over fresh water [*Wesely*, 1981] and 0.01 cm s^{-1} [*McKay et al.*, 1992] up to 0.05 cm s^{-1} over sea [*Lenschow et al.*, 1982]. *Galbally and Roy* [1980] presented a summary of results of measurements over sea and fresh water surfaces, indicating that surface resistances range from 1000 to 2000 s m^{-1}. Because of the small surface roughness length, R_{aX} will be larger over water compared to land surfaces. However, the surface resistance is still significantly larger compared to the aerodynamic resistance [*Lenschow et al.*, 1982]. Therefore introduction of an aerody-

namic resistance by application of (5) will not result in any significant temporal dependence of V_{dO3} over water surfaces. The current dry deposition scheme computes V_{dO3} over water surfaces using a value of r_{wat} of 2000 s m^{-1}. This value is also applied to snow and ice surfaces [*Galbally and Roy*, 1980; *Wesely*, 1981].

3.3.2. Nitric acid vapor. Over most surfaces the deposition velocity for gas phase HNO_3 is solely controlled by the aerodynamic resistance. This suggests that HNO_3 is deposited as rapidly as turbulent transfer allows [*Hanson and Lindberg*, 1991, and references therein]. Observed HNO_3 deposition velocities above crop canopies, deciduous forest, grass and other vegetation range from 0.5 to 26 cm s^{-1}, depending on vegetation type and windspeed. The vegetation resistance of HNO_3 is close to zero due to the high solubility and sticking coefficient, resulting in a small cuticle and mesophyll resistance. In contrast to O_3, the HNO_3 deposition velocity is therefore highly sensitive to the QBR [*Hanson and Lindberg*, 1991, and references therein; *Huebert and Robert*, 1985]. Deposition to water surfaces and soils can also be expected to be large. Parameterization of the surface resistances according to *Wesely* [1989] resulted in very small water and soil resistances. Furthermore, average HNO_3 deposition velocities above water/soil surfaces are rather small because of the small surface roughness. HNO_3 deposition velocities above snow observed by *Johannson and Granat* [1986] show a dependence on the snow temperature with a typical value of about 0.6 cm s^{-1} for a snow temperature of -2°C, decreasing rapidly to about 0 with decreasing snow temperatures [*Hanson and Lindberg*, 1991]. The physical mechanism responsible for this is unclear. In our scheme, the deposition velocity above all surfaces except for snow and ice, is calculated assuming a minimal surface resistance of 10 s m^{-1} in order to avoid unrealistic large deposition velocities over rough surfaces [*Wesely*, 1989]. This threshold deposition velocity is required for the scheme since the large-scale model surface roughness is dependent on the orography, resulting in very small aerodynamic resistances above mountainous regions. The HNO_3 surface resistance for snow and ice surfaces is calculated from the model's surface temperature, according to the relationship by *Wesely* [1989], based on the observations by *Johannson and Granat* [1986].

One should bare in mind that only the dry deposition of gaseous HNO_3 is calculated by our scheme. In reality some HNO_3 is removed from the lower troposphere by gas-to-particle conversion of HNO_3 and subsequent removal of aerosol nitrate. However, the latter process has not yet been incorporated in the chemistry scheme. For more information concerning the calculation of wet deposition of HNO_3 in the chemistry scheme we refer to *Roelofs and Lelieveld* [1995].

3.3.3. Nitrogen oxides. The dry deposition description for NO_x is relatively complicated compared to O_3 since the surface can be a sink as well as a source of NO. Results of field experiments have indicated that observed fluxes and concentrations of NO_x are not in agreement with flux-resistance relationship expressed by (2) and (3). Emission of NO is probably one of the causes of the disagreement. Another cause is violation of the constant flux approximation. The timescale of the chemical reactions of NO_x may be small compared to that of diffusive transport, resulting in local sources or sinks of NO_x and possibly flux divergence [*Kramm et al.*, 1993]. The applicability of the aerodynamic resistance using (4) for calculation of the NO_x deposition velocity seems therefore doubtful for the height of the model's lowest layer (~60 m). However, for most surfaces, the aerodynamic resistance is relatively small compared to the surface resistance and thus the error in the calculated deposition velocity will also be small. Concerning the surface resistance, in this work, representative resistances are selected to account for the sources. A more realistic representation of the interaction between emission and deposition has not been applied yet since the NO emission has been calculated in a separate routine of the chemistry model.

Vegetation: The dry deposition of NO_2 to vegetation is controlled by the stomatal aperture [*Hanson and Lindberg*, 1991; *Neubert et al.*, 1993], suggesting that there is no significant mesophyll resistance. However, deposition of NO_2 to broadleaf plant species appears to exceed that of coniferous species by a factor of 3–10 which can not be attributed to a difference of typical LAI values for these plant species alone. It was suggested by *Johansson* [1987] that a mesophyll resistance exists for coniferous trees, which comprises at least 50% of the total resistance to diffusion [*Hicks et al.*, 1989]. *Johansson* [1987] observed that the relationship between stomatal behaviour and uptake broke down with decreasing concentrations (Scots Pine). This suggests the existence of a "compensation point," the concentration for which emission balances deposition, and an increasing contribution of the mesophyll resistance into the total leaf resistance. The observed mesophyll resistance ranged from 10 to about 800 s m^{-1} [*Johansson*, 1987]. The existence of a compensation point for NO_2 concentrations of about 1–3 ppbv was also observed for Spruce trees by *Thoene et al.* [1991]. The existence of a mesophyll resistance for NO_2 is a possible explanation for observed differences in O_3 and NO_2 deposition velocities [*Wesely et al.*, 1982; *Delany and Davis*, 1983], the latter being about 2/3 of the O_3 deposition velocities. This difference between deposition velocities of O_3 and NO_2 can not be explained by different O_3 and NO_2 cuticle resistances. The cuticle NO_2 uptake plays a minor role, the cuticular uptake rate for NO_2 being at least 1–2 orders of magnitude less than representative rates to tree foliage through stomata [*Hanson and Lindberg*, 1991; *Kerstiens and Lendzian*, 1989; *Kramm et al.*, 1993]. In our deposition scheme, the mesophyll resistance for NO_2 is assumed to be half the leaf stomatal resistance, in order to calculate a NO_2 deposition velocity of about 2/3 the O_3 deposition velocity above vegetated areas, ignoring the difference of a broadleaf and coniferous plant mesophyll resistance. Calculating the mesophyll resistance from the stomatal resistance indirectly implies a dependence of the mesophyll resistance on light intensity, in agreement with observations by *Neubert et al.* [1993]. *Kramm et al.* [1993] proposed a correction term, depending on atmospheric and internal concentrations and resistances. This correction term may be accounted for in future versions of our deposition scheme if more detailed information concerning the 'compensation point' of other vegetation types becomes available. As long as this correction has not been made, a representative resistance must be chosen for the coexistence of emission and deposition. The cuticle resistance for O_3 (10^5 s m^{-1}) has also been adopted for NO_2.

There is little information available about the uptake of NO by plants. Uptake rates of NO observed by *Neubert et al.* [1993] are about one order of magnitude lower that those for NO_2, consistent with the findings reviewed by *Hanson and Lindberg* [1991]. The main reason for this significantly smaller deposition velocity is the relative large mesophyll resistance for NO [*Neubert et al.*, 1993, *Wesely*, 1989]. *Kisser-Priesack et al.* [1987] concluded, based on measurements with radioactively labelled

Table 1. Selected Soil, Cuticle, Mesophyll, Water, Snow/Ice Resistances for O_3, HNO_3, and NO/NO_2

	r_{soil}	r_{cut}	r_{mes}	r_{wat}	$r_{snow/ice}$
O_3	400	10^5	0	2000	2000
HNO_3	10	0	0	10	$\max(10, f(T_{surf}))$
NO_2	600	10^5	$0.5*r_{stom}$	10^5	10^5
NO	10^5	10^5	$5*r_{stom}$	10^5	10^5

Resistances are in seconds per meter.

NO, that cuticular uptake should not be ignored [*Hanson and Lindberg*, 1991, and references therein], also because of the relatively small loss by deposition through the stomata. In contrast, *Neubert et al.* [1993] and *Wesely* [1989] find that the uptake of NO by the cuticle does not contribute significantly to the foliage uptake. In our scheme, the mesophyll resistance for NO is assigned a 10 times larger value than that of NO_2, and for the cuticle resistance of NO we assumed the same value as for O_3 and NO_2.

Soil: Conductances to different soil types, as presented by *Hanson and Lindberg* [1991], indicate average soil resistances for NO_2 and NO of about 250 and 950 s m^{-1}, respectively. *Wesely* [1989] derived larger soil resistances for both trace gases. In the dry deposition scheme a value of 600 s m^{-1} is used for NO_2, resulting in NO_2 deposition velocities of 2/3 of the O_3 deposition velocity over vegetated areas (see equation (7)). This value of 600 s m^{-1} is probably reasonably representative for soils covered by vegetation since all the NO_2 soil conductances in the work by *Hanson and Lindberg* [1991] were determined in enclosure experiments. It can be expected that turbulent transfer in these chambers was optimal, contrary to the conditions in the canopy for which an additional resistance against turbulent transfer through the canopy to the soil surface should be adopted. Furthermore, high-exposure concentrations were used in the enclosure experiments. It can be expected that for typical tropospheric surface layer NO_2 concentrations, a representative soil resistance will be larger because of a more significant contribution of NO emission. This effect is more pronounced for NO since emission dominates deposition [*Stocker et al.*, 1993]. Therefore NO deposition to soils has been neglected.

Water, snow, and ice: As for O_3, the uptake of NO and NO_2 is limited by uptake into the aqueous phase and/or reaction with dissolved components [*Lee and Schwartz*, 1981; *Schwartz*, 1992]. The Henry's law constants for O_3 and NO_2 are comparable but the difference in reactivity results in a relatively larger uptake resistance for NO_2 for sea and fresh water. The Henry's law constant for NO is smaller than that of O_3, and NO is not significantly reactive in the aquous phase [*Wesely*, 1989; *Lee and Schwartz*, 1981]. In the dry deposition scheme, a value of 10^5 s m^{-1} is adopted for the sea and fresh water resistance of NO_2 and NO. An exact definition is not required since the dry deposition process to water remains very slow compared to gas phase reactions of NO and NO_2 [*Lee and Schwartz*, 1981]. Observed deposition velocities of NO_x over snow are less than 0.03 cm s^{-1} [*Granat and Johansson*, 1983]. *Valdez et al.* [1987] observed an average NO_2 deposition velocity to snow of about 0.01 cm s^{-1}. On the basis of these results and the relatively slow deposition process, a value of 10^5 s m^{-1} has been adopted for the snow and ice resistances for NO_x. Table 1 shows all the adopted resistances as used in this study.

4. Results

We present model simulations for the months January and July, for which strong differences in deposition velocities, associated with vegetation activity, chemistry, and meteorology, can be expected.

4.1. Diurnal Cycle and Comparison With Observations

Evaluation of the model against experimental results is difficult due to the large difference in spatial resolution of measured and model derived deposition velocities. The version of ECHAM model used (T21) has a spatial resolution of 5.6° × 5.6° (500–600 km at midlatitudes), while measured deposition velocities are site specific with typical spatial scales of about 0.1–1 km. In ECHAM, surface characteristics, for example, canopy structure, canopy height, LAI and vegetation type, are only coarsely represented. Therefore evaluation of V_{dX} is restricted to qualitive comparisons of diurnal and seasonal cycles, which are not very sensitive to the specific surface parameters but which are to a large extent controlled by turbulence and irradiance (e.g., through stomatal uptake). Further, evaluation of calculated NO_x and HNO_3 deposition velocities is limited by the relatively small amount of representative dry deposition data available.

Evaluation of V_{dO3} is most relevant for grid squares covered by vegetation or bare soil. For vegetated grid squares, both the surface and the aerodynamic resistance are computed from ECHAM parameters. Although bare soil surfaces have been assigned a constant surface resistance, the aerodynamic resistance still has a significant influence on V_{dO3} due to the relatively small surface roughness. Evaluation of V_{dO3} over water, snow and ice is of lesser importance because V_{dO3} merely depends on the assigned values of the relatively large surface resistance. Figures 1a–1h show the calculated monthly average diurnal cycle of V_{dO3} for six grid squares with typical vegetation classes for January and July. The grid squares are selected based on the distribution of major ecosystems [*Henderson-Sellers et al.*, 1986] and available observations of O_3 deposition velocities under comparable conditions (season, vegetation cover). Many available observations could unfortunately not be used because these observations were carried out over very different vegetation compared to the assigned vegetation class of the grid square. Figure 1a shows the diurnal cycle of V_{dO3} for north-western Europe. There is a distinct difference between the two months (seasons), resulting from the differences in stomatal and aerodynamic resistances. The January and July average diurnal cycles of r_{stom} and R_a for this grid square are shown in Figures 2a and 2b. The r_{stom} is large for January ($\approx$2000 s m^{-1}) and thus not shown. The deposition velocity is determined mostly by the soil resistance and R_a. The January diurnal cycle in V_{dO3} is less pronounced than in July since it is solely determined by R_a, which does not have such a large

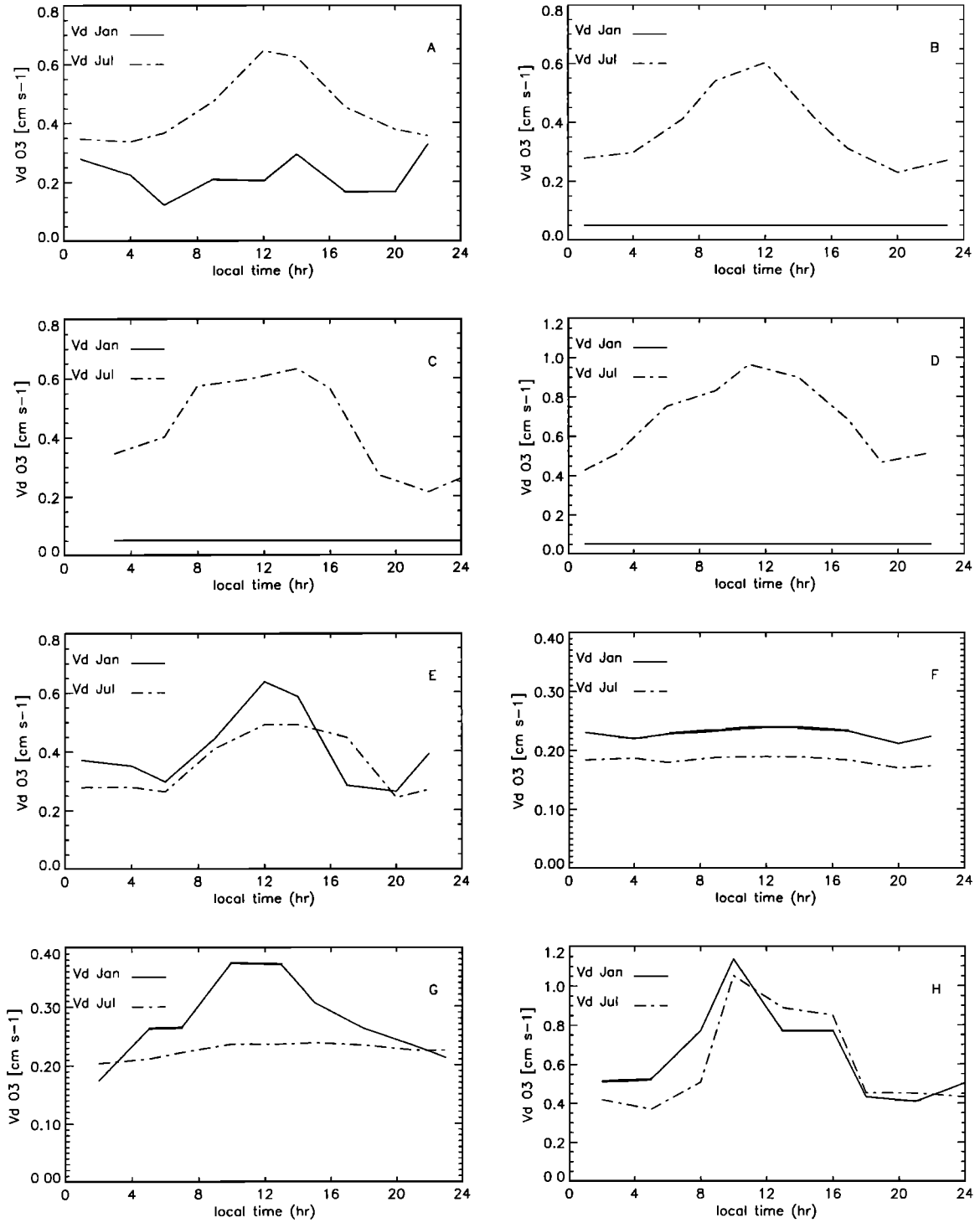

Figure 1. Monthly average diurnal cycle of V_{dO3} for January and July, (a) northwestern Europe, 55° N, 10° E, the vegetation class is crop, (b) northeastern Canada, 55° N, 65° W, vegetation class evergreen tree, in January V_{dO3} has a constant value of 0.05 cm s^{-1} as a result of snow cover, (c) east Canada, 45° N, 80° W, vegetation class deciduous tree, snow cover in January, (d) Alaska, 60° N, 150° W, vegetation class tundra/desert, snow cover in January, (e) western North America, 40° N, 115° W, vegetation class grass and shrub, (f) north Africa, 20° N, 15° E, vegetation class tundra/desert, (g) Australia, 30° S, 140° E, vegetation class grass and shrub, and (h) South America, 5° S, 45° W, vegetation class evergreen tree.

amplitude in the daily variation as the stomatal resistance. The average V_{dO3} in northwestern Europe in January is about 0.25 cm s^{-1}, approximately the inverse value of r_{soil}. In July, r_{stom} is at maximum during nighttime whereas a high R_a additionally limits transfer of O_3 through the atmosphere as a result of the stable stratification. The diurnal cycle of r_{stom} is very similar to the diurnal cycle of V_{dO3}. The inverse value of r_{stom} does not differ much from the absolute level of V_{dO3} which means that

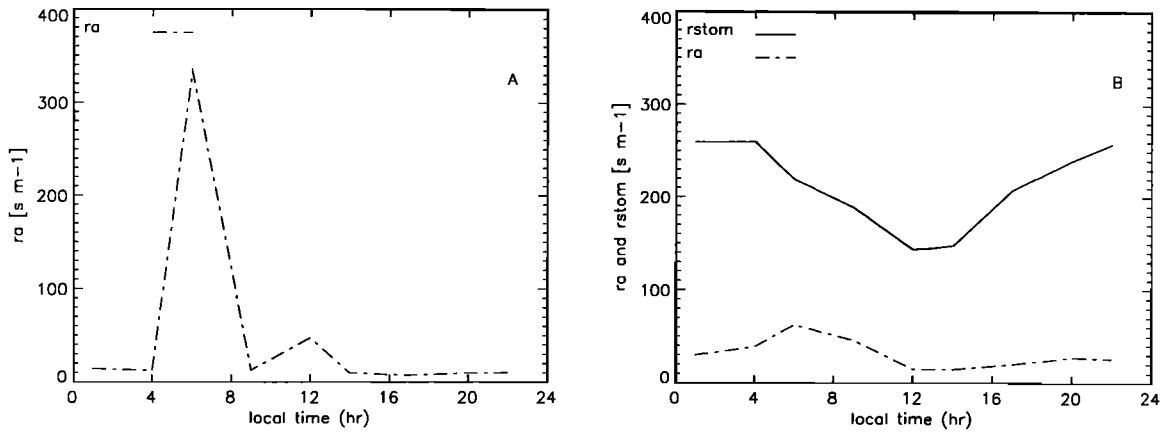

Figure 2. Monthly average diurnal cycle of R_a and r_{stom} for O_3 of northwestern Europe for (a) January ($r_{stom} \approx 2000$ s m^{-1}, not shown here) and (b) July.

V_{dO3} is largely controlled by r_{stom}. R_a has no significant limiting effect on V_{dO3}. The QBR is not presented in Figures 2a and b because of its relatively small value. A sensitivity study indicated that the average R_a is about 1 order of magnitude larger than the QBR, which implies that no elaborate description of the QBR is required for these conditions.

Table 2 shows daily average, maximum and minimum calculated O_3 deposition velocities and a selection of observations over comparable surfaces and season. No observed diurnal cycles are presented here, however, the diurnal and seasonal cycles are dependent on the same quantities, which are represented by their average, maximum and minimum values. The agreement between calculated and observed O_3 deposition velocities appears to be satisfactory. The calculated V_{dO3} over all surfaces, except for the deserts of North-Africa and South-American forests, shows a distinct difference between the two months. There is a diurnal cycle in V_{dO3} for all surfaces in the summer and winter except for the snow covered surfaces (a V_{dO3} of about 0.05 cm s^{-1} in January in Figure 1b, 1c, and 1d) and the deserts. The small seasonal and diurnal cycles over deserts are related to the negligible vegetation influence on the deposition process. The average V_{dO3} of 0.25 cm s^{-1} approximates the inverse value of the assigned soil resistance since the aerodynamic resistance does not significantly contribute to V_{dO3} despite the relatively small surface roughness. The overestimation of V_{dO3} by the model over tundra in Alaska can probably be attributed to the fact that ECHAM does not contain a representation of inland water while the measurements were carried out over relatively wet tundra terrain [*Jacob et al.*, 1992; *Ritter et al.*, 1992]. The V_{dO3} over western North America in July is smaller than in January as a result of the reduced stomatal uptake due to water stress. The daytime V_{dO3} over tropical forest is underestimated by the model which indicates that the scheme does not succeed in simulating the very efficient stomatal uptake by tropical forest.

4.2. Global Distribution of Deposition Velocity, Deposition, and Concentrations

Ozone: Figures 3a and 3b show the January and July average global V_{dO3} distribution, indicating a distinct spatial distribution over the continents, which is mostly related to differences in surface characteristics. In July, relatively large values of V_{dO3} occur in the areas with dense vegetation cover, for example, the temperate forests in the northern hemisphere

Table 2. Comparison of Calculated and Observed V_{dO3} Values Above Comparable Surfaces Under Comparable Conditions

Figure Number and Deposition Surface	Calculated V_{dO3}, cm s^{-1} average (maximum, minimum)	Reference, Observed V_{dO3}, cm s^{-1} average (maximum, minimum)
1a: crop, northwestern Europe	Jan. 0.2 (0.3,0.15)	
	July 0.5 (0.65,0.35)	*Van Pul* [1992], 0.46 (≈0.6, ≈0.35)
1b: evergreen tree, northeastern Canada	Jan.0.05(snow)	
	July 0.4 (0.6,0.25)	*Ritter et al.* [1994], 0.4 (0.65, 0.25)
1c: decidious tree, east Canada	Jan.0.05(snow)	*Padro et al.* [1993], ≈0.2 (0.3, 0.1), ≈0.6 (1.25, 0.25)
	July0.45 (0.65,0.25)	
1d: tundra, Alaska	Jan.0.05(snow)	*Sehmel* [1980], 0.7*
	July 0.7 (1.0, 0.4)	*Jacob et al.* [1992] and *Ritter et al.* [1992], 0.2 (0.35, 0.1)
1e: grass and shrub, western North America	Jan. 0.4 (0.65,0.25)	
	July0.35 (0.5,0.25)	*Massman et al.* [1994], 0.3 (0.5, 0.1)
1f: tundra and desert, north Africa	Jan.0.25	*Sehmel* [1980], ≈0.30*
	July0.25	
1g: grass and shrub, Australia	Jan. 0.3 (0.4, 0.2)	*Sehmel* [1980], 0.4 (0.6, 0.2)*
	July 0.2	
1h: evergreen tree, South America	Jan. 0.8 (1.15, 0.4)	*Fan et al.* [1990] ≈1.0 (≈2.5, ≈0.25)*
	July 0.8 (1.0,0.35)	

*Yearly average V_{dO3} and values between parentheses denote maximum and minimum V_{dO3}.

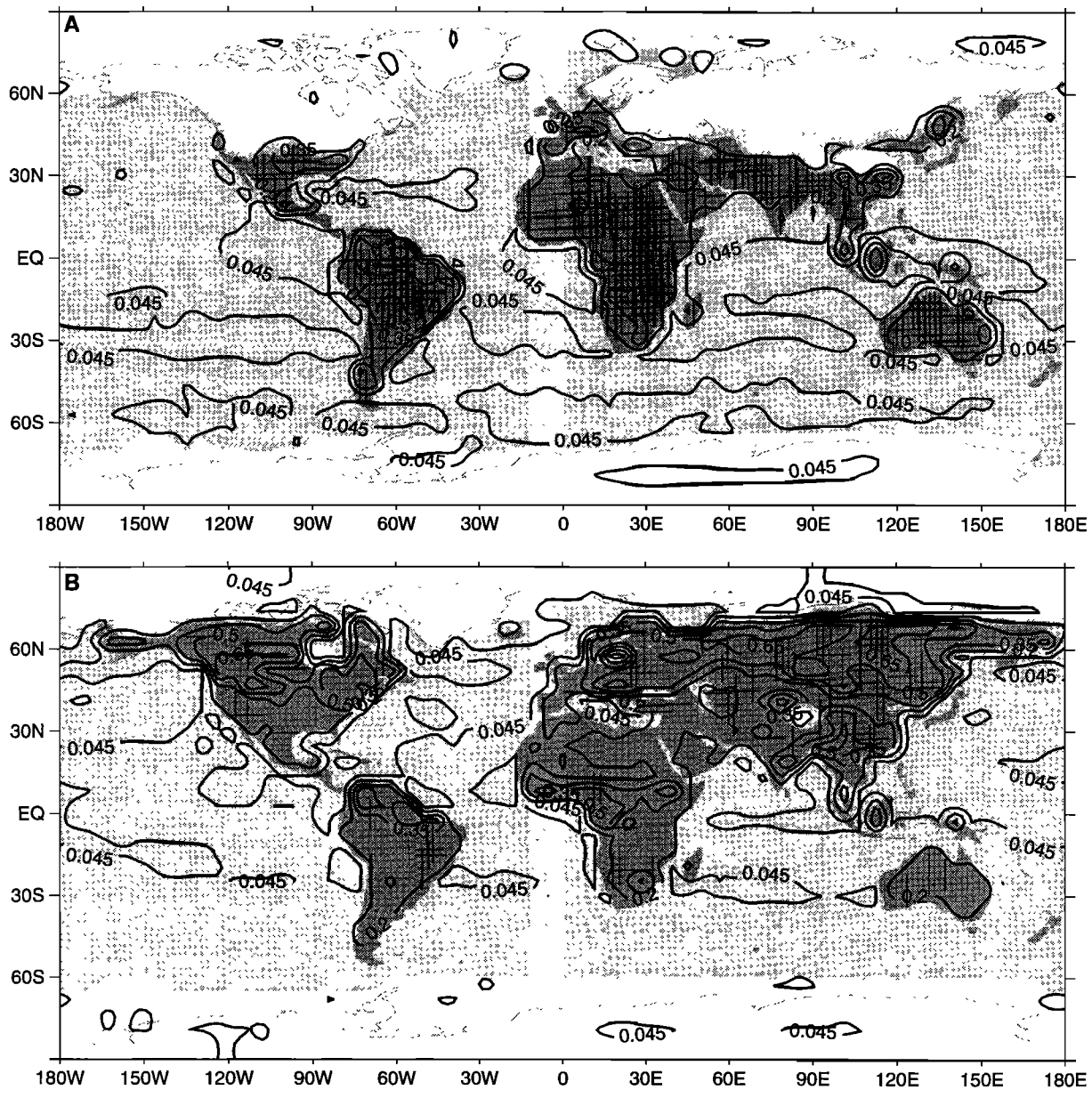

Figure 3. Monthly average O_3 deposition velocity (cm s^{-1}), (a) January, (b) July. Ice and snow cover is represented by the white color. The isolines are 0.045, 0.2, 0.35, 0.5, and 0.65.

(NH) and forested regions in the tropics. Relatively small deposition velocities of about 0.1–0.2 cm s^{-1} are calculated over the deserts of Africa and the Middle East. In the southern hemisphere (SH), V_{dO3} values are relatively small, with values of about 0.2 cm s^{-1} in Australia, and 0.25 cm s^{-1} in large parts of South America and Africa. Figures 3a and 3b also indicate the seasonal differences in V_{dO3} over the continents. The values of V_{dO3} in January are quite different from those in July, being very small over North America and northern Europe and Siberia in January, caused by the snow cover in these areas. Over sea, V_{dO3} is about 0.05 cm s^{-1}. Relatively low wind speeds and consequently small surface roughnesses in subsidence areas, following the Hadley cell circulation, result in somewhat increased aerodynamic resistances in the subtropics in both hemispheres.

The results of our deposition scheme have been compared with those of a scheme in which V_{dO3} was kept at a constant value (hereafter referred to as "constant V_{dO3}" scheme) of 0.35 cm s^{-1} over land (without snow/ice cover) which was used previously in a global model by *Dentener and Crutzen* [1993], and 0.05 cm s^{-1} over sea and snow/ice surfaces. Figure 4a shows the relative differences between O_3 deposition, calculated as (new scheme minus "constant V_{dX}" scheme)/("constant V_{dX}" scheme). Especially over vegetated areas, ozone deposition increases by 10–50% over the NH. The new deposition scheme calculates less O_3 deposition over arid regions, for example, the African and Middle East deserts and Australia. Reductions of O_3 deposition over the oceans are caused by introduction of the aerodynamic term, thereby increasing the total resistance with about 200–500 s m^{-1}. The relative differences between the monthly average O_3 concentrations in the surface layer by both schemes for July are given

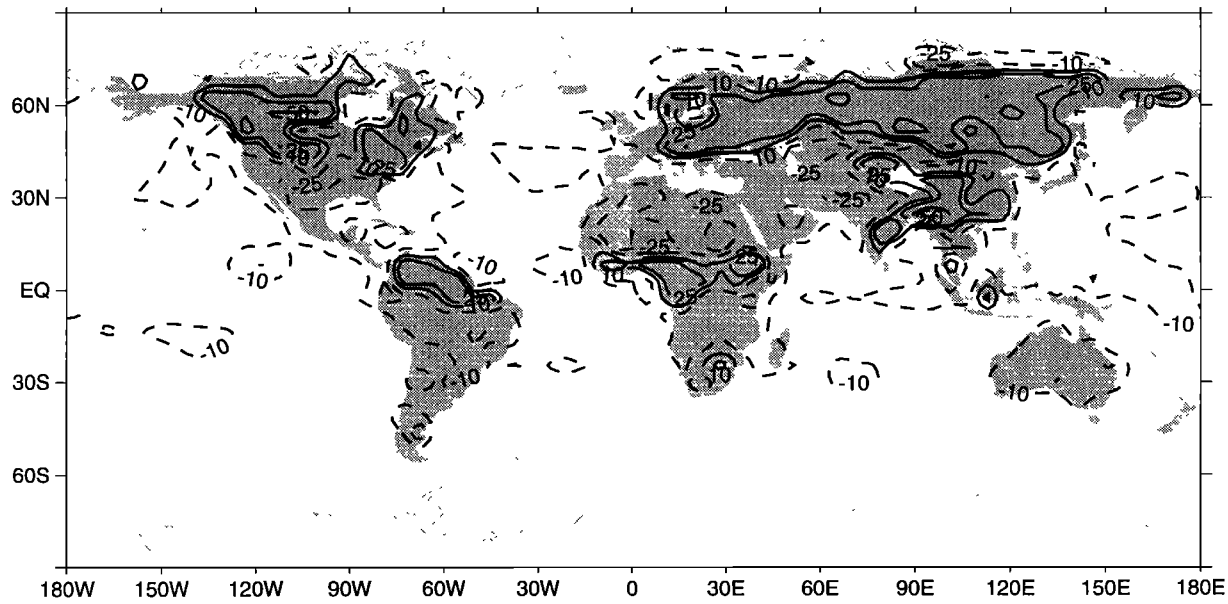

Figure 4a. Relative difference (percent) of O_3 deposition between the new dry deposition scheme and the "constant V_{dO3}" scheme, July. Dashed and solid lines indicate a decrease and increase, respectively, of deposition calculated by the new scheme compared to the "constant V_{dO3}" scheme. The isolines are −25, −10, 10, 25, and 50.

in Figure 4b. These are generally smaller than the differences in O_3 deposition, associated with negative feedbacks in O_3 concentration changes through dry deposition and chemistry. However, nonnegligible O_3 concentration differences occur (~5%) between the two schemes up to an altitude of about 1.5–2 km.

Nitric acid vapor: Figure 5 shows the January average global V_{dHNO3} distribution. The V_{dHNO3} over all surfaces, except snow/ice covered surfaces, is controlled by turbulent transfer. The limiting influence of the surface temperature dependent snow/ice resistance is clearly visible in Canada and Russia. Very large V_{dHNO3} values, up to 7.5 cm s^{-1}, occur in mountainous regions as a result of a large surface roughness. Over land, V_{dHNO3} exceeds 2 cm s^{-1} over large areas, while over sea the calculated V_{dHNO3} ranges between about 0.4 cm s^{-1} in subsidence areas and 1.6 cm s^{-1} in areas with large windspeeds. Figure 6 shows the relative differences between the January average HNO_3 concentrations in the model's surface layer with the "constant V_{dHNO3}" scheme (V_{dHNO3} is 0.8 cm s^{-1} over sea/snow/ice and 2 cm s^{-1} over land, as used by *Dentener and Crutzen* [1993]) and the new scheme. Relative decreases in HNO_3 concentrations calculated with the new scheme compared to the "constant V_{dHNO3}" scheme are as

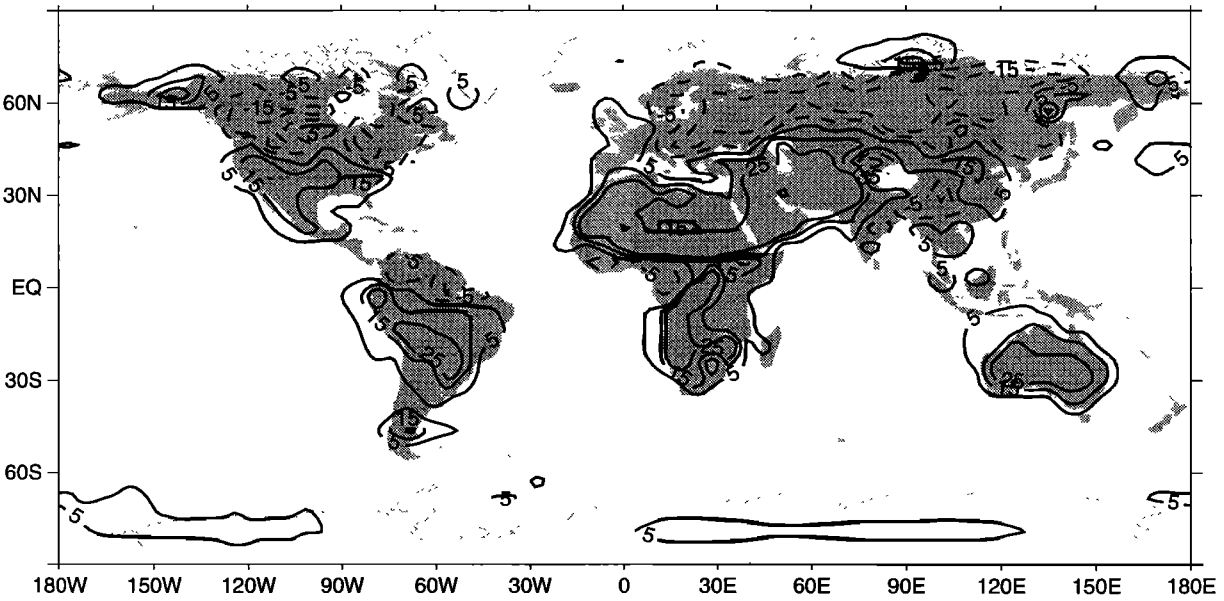

Figure 4b. Relative difference (percent) of the O_3 surface layer concentration between the new scheme and the "constant V_{dO3}" scheme (see Figure 4a), July. The isolines are −25, −15, −5, 5, 15, and 25.

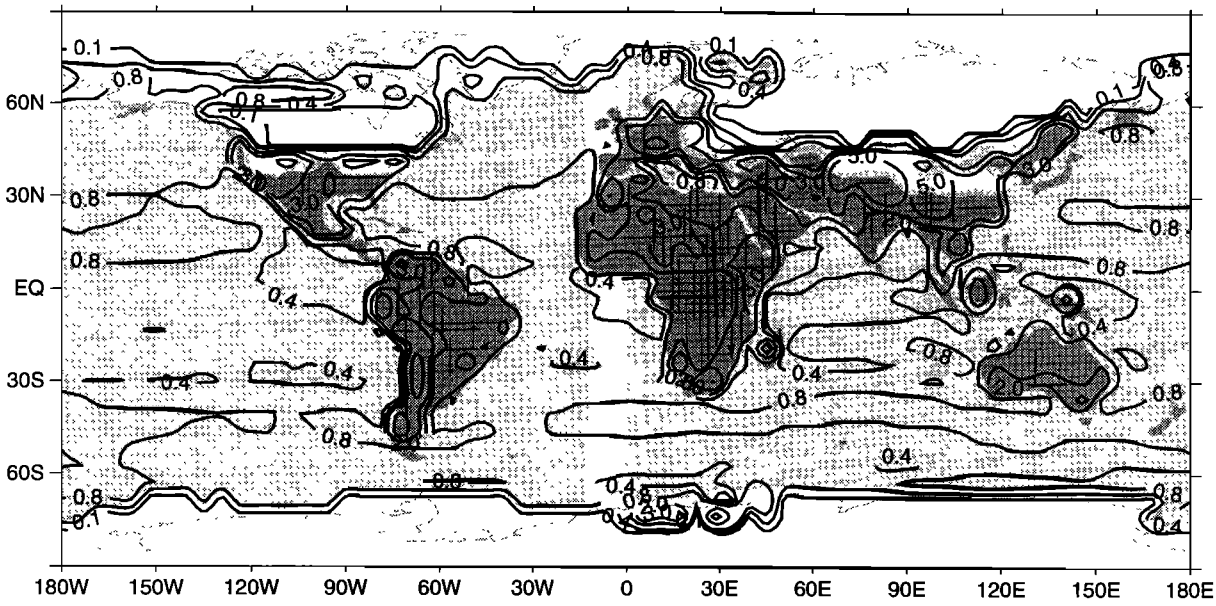

Figure 5. Monthly average HNO_3 deposition velocity (cm s^{-1}), January. The isolines are 0.1, 0.4, 0.8, 2.0, 3.0, and 5.0.

large as 25% in mountainous regions while relative increases up to 75% occur in subsidence areas over sea. At higher latitudes, over snow and ice, there is an increase in HNO_3 concentrations due to a relatively small V_{dHNO3} resulting from the large surface resistance. However, HNO_3 concentrations in these areas are relatively small and the contribution of the dry deposition to the global HNO_3 budget is negligible. Changes in HNO_3 dry deposition are counteracted by changes in wet deposition through concentration changes. In general, we calculate only small changes in the O_3 surface layer concentrations as a result of changes in HNO_3, comparing our dynamic and the "constant V_{dHNO3}" scheme.

Nitrogen oxide and nitrogen dioxide: The monthly average global $V_{dNO/NO2}$ distributions have similar global distribution patterns as V_{dO3}. The values of V_{dNO2} and V_{dNO} are about 2/3 and 1/10 those of O_3 above vegetation and bare soil, respectively. Over sea, $V_{dNO/NO2}$ is about 10^{-5} cm s^{-1} and does not show any significant diurnal or seasonal cycles. There are no significant relative differences in NO and NO_2 surface layer concentrations between our scheme and the "constant V_{dNOx}" scheme (V_{dNO} is 0 cm s^{-1} over sea/snow/ice and 0.04 cm s^{-1} over land, and V_{dNO2} is 0.1 cm s^{-1} over sea/snow/ice and 0.25 cm s^{-1} over land [*Dentener and Crutzen*, 1993]) although NO_x deposition fluxes change markedly (see section 4.3).

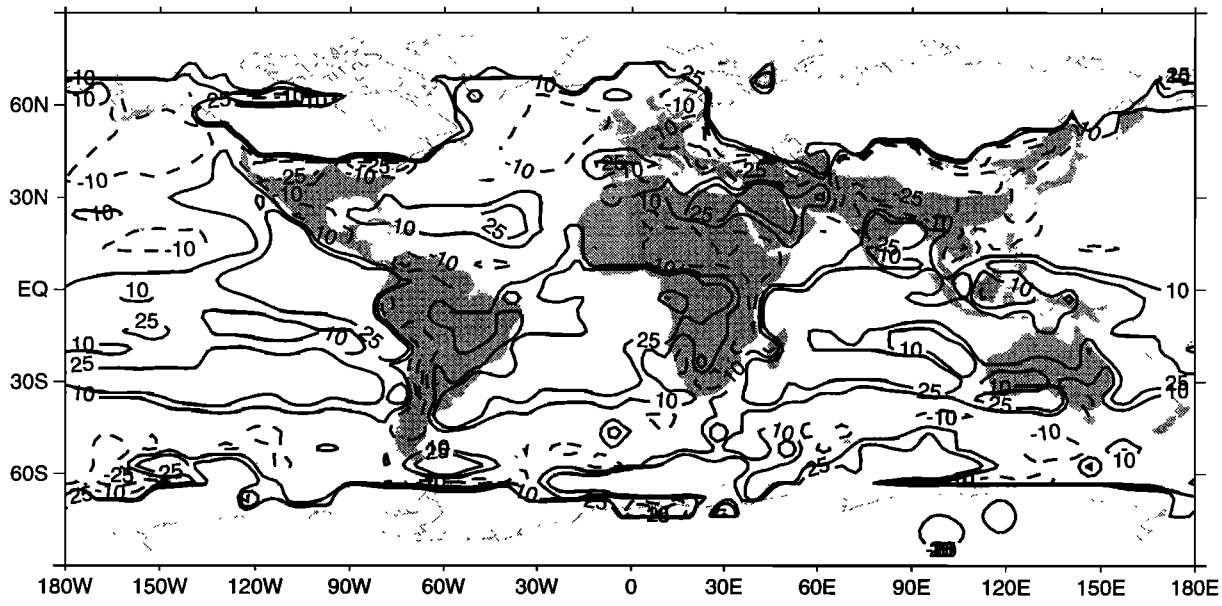

Figure 6. Relative difference (percent) of HNO_3 surface layer concentration between the new scheme and the "constant V_{dHNO3}" scheme (see Figure 4a), January. The isolines are −25, −10, 10, and 25.

Table 3. Relative Differences and Absolute Levels of O_3, HNO_3, and NO_x Dry Deposition in Four Approximately Equal Areas of the Globe Comparing the "Constant V_{dX}" Scheme and the New Dry Deposition Scheme

	O_3 (Tg O_3)		HNO_3 (Tg N)		NO_x (Tg N)	
	January	July	January	July	January	July
90°–30° N	0 (6.7)	7 (19.4)	−7 (0.17)	3 (0.74)	−29 (0.46)	15 (0.36)
30°–0° N	−10 (15.1)	−7 (15.8)	0 (0.39)	−2 (0.53)	−8 (0.21)	−2 (0.13)
0°–30° S	3 (8.9)	−10 (10.7)	3 (0.25)	2 (0.37)	3 (0.08)	−10 (0.17)
30°–90° S	−6 (1.3)	−5 (3.5)	0 (0.01)	13 (0.02)	0 (0.00)	−17 (0.01)
Global	−4 (31.9)	−2 (49.5)	−3 (0.82)	1 (1.65)	−20 (0.75)	4 (0.67)

Differences are in percent. Values in parentheses are absolute levels. Positive values indicate an increase in deposition calculated by the new scheme compared to the "constant V_{dX}" scheme.

These changes are balanced, however, by feedbacks in the chemistry.

4.3. Global Changes Due to the New Scheme

Table 3 shows the relative differences and the absolute levels of O_3, HNO_3, and NO_x deposition in four approximately equal areas of the globe (0°–30° and 30°–90° N and S), comparing the new scheme and the "constant V_{dX}" scheme for January and July (for the calculation of relative differences, see section 4.2). Relative differences of dry deposition in the NH are up to 10% for O_3, 7% for HNO_3, and 29% for NO_x. The dry deposition of O_3 and NO_x shows a distinct difference between January and July due to a dependency on surface characteristics and vegetation activity. The relative differences integrated over the entire globe are small for O_3 and HNO_3. Application of our new deposition scheme for NO_x is most significant for the NH, where dry deposition decreases in winter and increases in summer. Although the differences in trace gas deposition and surface layer concentrations on a global scale may not seem dramatic, regional differences can be significant. Moreover, the new scheme contributes to internal consistency of the model, in particular with respect to diurnal and seasonal cycles in the chemistry, turbulent exchange processes and surface characteristics that control dry deposition.

5. Discussion

The new model routine presented improves the calculation of deposition velocities at different locations with various coverages. However, there are still shortcomings which need to be improved in future versions. Some uncertainties involving the calculation of R_{aX}, and R_{surf} are discussed next.

Uncertainties in R_{aX}: One possible error in R_{aX} is introduced by the violation of the constant flux layer approach for reactive trace gases. Chemical transformations can modify the local turbulent transfer rates if the time scale for chemical reactions is much smaller than that of turbulent diffusion. Photochemical reactions between NO/NO_2 and O_3 can be quite rapid, with time scales comparable to those of turbulent transfer at a height of 1 m above the surface. For example, in regions with strong NO emissions, titration of O_3 can be significant. Above ≈1 m, the timescale of turbulent transfer increases with height, so that chemical reactions can become increasingly important in the surface layer [*Gao et al.*, 1991]. The aerodynamic resistance, calculated at the model's reference height of 30 m through (4), might therefore not be representative for the turbulent transfer of these trace gases from this reference height to the surface. If the aerodynamic resistance significantly contributes to the total resistance, ignoring the effects of chemical reactions on deposition velocities of NO and NO_2 may cause errors. However, under most conditions the effects of rapid chemical reactions on the O_3 deposition velocities are expected to be small [*Gao et al.*, 1991]. Violation of the constant flux approach can become significant in regions with relatively small surface roughness, for example, water, snow, ice, bare soil, and vegetated surfaces with low canopies. However, these regions mostly do not have strong NO emissions. Future studies should focus on the relevance and a possible solution of this problem since chemistry and transport calculations are not treated simultaneously in the model.

A second source of errors in calculating R_{aX} is the use of ECHAM's surface roughness for momentum (z_{0m}) as a substitute for that of trace gases. In the current version of the model, z_{0m} also accounts for the large scale orography, in addition to the representation of local surface roughness. This results in extremely large z_{0m} values for some locations (20 m). In this work, a correction for differences between z_{0m} and z_{0X} has been applied by defining a QBR. However, a more representative ratio of z_{0m} and z_{0X} may be used in the calculation of the QBR (see equation (5)), or the definition of a representative local surface roughness to compensate for overestimation of R_{aX} over regions with a large z_{0m}. Changing the surface roughness from its original value of 0.2 m (surface roughness for northwestern Europe), to 5 m resulted in average relative difference in V_{dO3} of 11% with maximum relative differences of about 40%. In ECHAM, areas in the western part of South America, Central America, and the Himalaya, have large surface roughnesses of 5–15 m, causing very large deposition velocities, especially for HNO_3. In southern South America the scheme computes relatively large O_3 deposition velocities, even though the surface resistance is relatively large, which can be attributed to a large surface roughness and a small R_{aX}. Hence, in future versions of the scheme the model surface roughness description must be improved for dry deposition calculations.

A possible bias in the model, related to the definition of the surface roughness, is the use of ECHAM's reference height of the lowest layer (≈30 m) as reference height for the dry deposition velocity. For small surface roughness and stable conditions the reference height might be higher than the constant flux layer while for very large surface roughnesses, the reference height might be located within the roughness layer; in both cases this results in a violation of the constant flux ap-

proach. However, we think that based on the relatively small area with large surface roughness (>2 m), the small contribution of the deposition during stable events in the total deposition, and a height of the constant flux layer of about 50 m during daytime, using ECHAM's reference height is a good compromise between maintaining consistency in the model and minimizing possible errors.

An additional source of uncertainty is the neglect of a representative local displacement height (see equation (4)) in our model which would be more appropriate to use for trace gas exchange. Information concerning the canopy structure is restricted to the LAI and the vegetation ratio. The canopy height of each vegetation class, which could be used to estimate a local displacement height d, is not defined in the model. Sensitivity analysis indicates that $V_{d\mathrm{HNO3}}$, which is largely controlled by R_{aX}, increases about 15% for an (extreme) increase in d of 15 m. The relative errors in the O_3 and NO/NO_2 deposition velocities are small (~2%).

Uncertainties in R_{surf}: As a consequence of the coarse grid resolution of the model, there are large uncertainties in factors which control the surface resistance. One aspect is the small selection of different vegetation classes. It is shown in the results, based on the comparison of calculated and observed O_3 deposition velocities, that a more sophisticated distinction should be made between different vegetation classes, for example, tropical forest and evergreen trees. The canopy structure is crudely defined in the ECHAM model, for example the LAI and canopy height for different vegetation classes are not distinguished. The seasonal cycle in the vegetation fraction is only coarsely represented (only winter and summer values), while the LAI is assumed to be constant throughout the year for all vegetation classes. The constant LAI of 4 is used for upscaling the leaf resistance to a foliage resistance in this version of the dry deposition model for internal model consistency. However, due to shade effects and the extinction of turbulence within a canopy, linear scaling with LAI is inaccurate for LAI larger than 2–3. Furthermore, the LAI is used to determine the bulk canopy resistance (equation (7)), resulting in a nonvariable contribution of the soil resistance to the bulk resistance for all vegetation classes. Sensitivity analysis, using an LAI of 1 instead of 4, showed a relative difference in the V_{dO3} of 10–20%. Improvement of the LAI representation, for example, adapting seasonally representative LAI values for a more appropriate selection of different vegetation classes, will be involved in the future. An advancement planned in the representation of the canopy structure, expressed by the LAI, a local displacement height and local surface roughness, will be the use of the Olson vegetation data set [*Olson et al.*, 1985] in which the distribution of 46 global ecosystems and their characteristics are defined.

Further, the compensation point in the NO_2 uptake process by vegetation may be improved in future versions of our scheme. *Johansson* [1987] observed NO_2 emissions from Scots Pine in enclosure experiments at concentrations below the compensation point of 1-3 ppb. In the model, coniferous forests cover large areas of Alaska, Canada, northern Europe and northern Russia, while calculated NO_2 concentrations in the surface layer during July are less than 1 ppb over these areas. If the compensation point as observed by *Johansson* [1987] and *Thoene et al.* [1991] is representative for coniferous forests, more NO_x will remain in the atmosphere over these areas since dry deposition may be negligible whereas emissions of NO are conceivable.

The effect of foliage wetness on the deposition process has been investigated in several recent dry deposition studies [*Baldocchi*, 1993; *Chameides*, 1987; *Fuentes et al.*, 1992; *Wesely*, 1989]. For example, deposition of HNO_3 to a wetted foliage is entirely determined by R_{aX} [*Chameides*, 1987]. Foliage wetness might significantly alter the surface resistances of the less soluble trace gases NO_x and O_3. An enhanced O_3 deposition due to foliage wetness has been measured above a deciduous forest by *Fuentes et al.* [1992]. Their observations indicate that mechanisms, other than stomatal uptake contribute to the O_3 deposition when the foliage is wet. Various assumptions have been made in deposition models regarding the effect of foliage wetness on O_3 uptake. Early models assumed a decrease of the uptake of O_3 under wet conditions. More recent models make a distinction between foliage wetness caused by rain and by dew to account for their different chemical compositions [*Wesely*, 1989]. In our scheme, the effect of foliage wetness on dry deposition due to rain or dew has not be treated separately since foliage wetness in the ECHAM model (water in skin reservoir) is the net result of both processes. In future, a parameterization by *Chameides* [1987] may be incorporated, especially when the dry deposition scheme is extended to soluble trace gases such as SO_2.

The soil resistance for ozone of 400 s m^{-1} adopted in our scheme, may be relatively large. However, evaluation of the O_3 deposition velocities over vegetated surfaces indicates reasonable agreement between observed and calculated O_3 deposition velocities. Decreasing the soil resistance to about 100 s m^{-1}, a value often used in other schemes, would result in a too large V_{dO3} in absolute terms and in its amplitude in the diurnal cycle. The average V_{dO3} over sand is about 0.3 cm s^{-1} [*Sehmel*, 1980], while the calculated V_{dO3} in the desert areas of North Africa and the Middle East ranges from about 0.25 up to 0.5 cm s^{-1}, which justifies the choice of r_{soil} = 400 s m^{-1} for ozone. The NO_x soil resistances adopted are debatable since these are based on observed exchange rates of NO_x which may represent the net effect of NO_x uptake and NO emission. NO deposition to soils is ignored and a soil resistance of 600 s m^{-1} has been adopted for NO_2, yielding a deposition velocity of 2/3 the O_3 deposition velocity over vegetation. Considering the uncertainties, the calculated NO_x deposition velocities over surfaces with significant soil uptake should be interpreted with care. It is important to improve the parameterization of the soil uptake process in future because the soil resistance basically determines the dry deposition during nighttime due to the large foliage resistance. Furthermore, introduction of an LAI seasonal cycle will result in an increased contribution of r_{soil} to the surface resistance during winter and for vegetation classes with small LAI values throughout the year. As for the canopy representation, soil data bases will be used to distinguish different soil types and this information will be combined with ECHAM parameters, for example, soil wetness, to calculate more representative soil resistances for different locations in future versions of the model.

The calculated HNO_3 snow/ice surfaces resistances should be evaluated using additional observations. The O_3 and NO_x deposition are relatively small because of the large water and snow/ice resistances. An exact definition of the NO_x water and snow/ice surface resistance is not required since the deposition process to water and snow/ice surfaces remains very slow compared to the gas phase reactions [*Lee and Schwartz*, 1981]. However, even with relatively low V_{dO3} values over these surfaces, the contribution of O_3 deposition in the overall budget is

still significant due to their large areal extent and relatively slow gas phase reactions. For a deposition velocity of about 0.05 cm s^{-1} and an average height of the model's lowest layer of 60 m, the time constant of dry deposition process is 1–2 days, while the average lifetime of ozone in lower troposphere is about 10 days. Thus deposition to water/snow/ice is very significant for the ozone budget of the lower troposphere. This emphasizes the need for a more sophisticated definition of the dry deposition process to these surfaces in future.

6. Conclusions

Even though considerable uncertainties remain, the dry deposition scheme calculates realistic deposition velocities of O_3, HNO_3, and NO_x over most locations for different meteorological conditions, consistent with diurnal and seasonal cycles in both the chemistry and the planetary boundary layer processes and surface characteristics that control dry deposition. This not only improves the overall model performance but also the possibility to compare the model output with experimental results since most measurements are performed at the surface. In general, we calculate distinct diurnal and seasonal cycles with relatively large deposition velocities during daytime and summer, and lower deposition velocities during nighttime and winter. Incorporation of the scheme in the chemistry general circulation model ECHAM yielded significant changes in the deposition fluxes and concentrations in the lower troposphere compared to a scheme using constant deposition velocities. For example, the new scheme calculates up to about 25% lower O_3 concentrations in the surface layer in the summertime continental NH. Dry deposition of HNO_3 is to a large extent controlled by the aerodynamic resistance R_a, while that of O_3 and NO_x is determined mostly by R_{surf}, that is, r_{soil} and r_{veg}. However, R_a is also strongly influenced by surface characteristics, which emphasizes the great importance of realistic representations of these parameters in future versions of the dry deposition scheme.

Acknowledgments. This work was performed within the SINDICATE project (Study on the Indirect and Direct Climate Influences of Anthropogenic Trace Gas Emissions). We thank the Deutsches Klimarechenzentrum/Max-Planck-Institut für Meteorologie in Hamburg, Germany, for the use of computer facilities and support. We also thank Erich Roeckner, Geert-Jan Roelofs, and Frank Dentener for discussions and comments.

References

Baldocchi, D. D., Deposition of gaseous sulfur compounds to vegetation, in *Sulfur Nutrition and Assimilation and Higher Plants*, edited by L. J. De Kok et al., pp. 271–293, SPB Academic, The Hague, Netherlands, 1993.

Baldocchi, D. D., B. B. Hicks, and P. Camara, A canopy stomatal resistance model for gaseous deposition to vegetated surfaces, *Atmos. Environ.*, *21*, 91–101, 1987.

Brutsaert, W., *Evaporation Into the Atmosphere*, Kluwer Academic, Norwell, Mass., 1973.

Chameides, W. L., Acid dew and the role of chemistry in the dry deposition of reactive gases to wetted surfaces, *J. Geophys. Res.*, *92*, 11,895–11,908, 1987.

Charnock, M., Wind stress on a water surface, *Q. J. R. Meteorol. Soc.*, *81*, 639–640, 1955.

Delany, A. C., and T. D. Davies, Dry deposition of NOx to grass in rural East Anglia, *Atmos. Environ.*, *17*, 1391–1394, 1983.

Dentener, F. J., and P. J. Crutzen, Reaction of N2O5 on tropospheric aerosols: Impact on the global distributions of NOx, O3, and OH, *J. Geophys. Res.*, *98*, 7149–7163, 1993.

Deutsches Klimarechenzentrum, Modellbetreuungsgruppe, The ECHAM3 atmospheric general circulation model, *Tech. Rep. 6*, Hamburg, Germany, 1992.

Dyer, A. J., and B. B. Hicks, Flux-gradient relationships in the constant flux layer, *Q. J. R. Meteorol. Soc.*, *96*, 715–721, 1970.

Fan, S.-M., S. C. Wofsky, P. S. Bakwin, D. J. Jacob, and D. R. Fitzjarrald, Atmosphere-biosphere exchange of CO2 and O3 in the Central Amazon forest, *J. Geophys. Res.*, *95*, 16,851–16,864, 1990.

Fuentes, J. D., T. J. Gillespie, G. den Hartog, and H. H. Neumann, Ozone deposition onto a deciduous forest during dry and wet conditions, *Agric. Forest Meteorol.*, *62*, 1–18, 1992.

Galbally, I. E., and C. R. Roy, Destruction of ozone at the Earth's surface, *Q. J. R. Meteorol. Soc.*, *106*, 599–620, 1980.

Gao, W., M. L. Wesely, and L. Y. Lee, A numerical study on the effects of air chemistry on fluxes of NO, NO2, and O3 near the surface, *J. Geophys. Res.*, *96*, 18761–18769, 1991.

Garratt, J. R., and B. B. Hicks, Momentum, heat and water vapour transfer to and from natural and artificial surfaces, *Q. J. R. Meteorol. Soc.*, *99*, 680–687, 1973.

Granat, L., and C. Johansson, Dry deposition of SO2 and NOx in winter, *Atmos. Environ.*, *17*, 191–192, 1983.

Hanson, P. J., and S. E. Lindberg, Dry deposition of reactive nitrogen compounds: a review of leaf, canopy and non-foliar measurements, *Atmos. Environ.*, Part A, *25*, 1615–1634, 1991.

Henderson-Sellers, A., M. F. Wilson, G. Thomas, and R. E. Dickinson, Current global land-surface data sets for use in climate-related studies, *Tech. Note, NCAR/TN-272+STR*, Natl. Cent. for Atmos. Res., Boulder, Colo., 1986.

Hicks, B. B., D. D. Baldocchi, T. P. Meyers, R. P. Hosker Jr., and D. R. Matt, A preliminary multiple resistance routine for deriving dry deposition velocities from measured quantities, *Water Air Soil Pollut.*, *36*, 311–330, 1987.

Hicks, B. B., et al., Atmospheric processes research and process model development, State-of-Science/Technology, *Rep. 2*, Natl. Acid Precip. Assess. Program, NOAA/ATDD contrib. 89/20, Oak Ridge, Tenn., 1989.

Huebert, B. J., and C. H. Robert, The dry deposition of nitric acid to grass, *J. Geophys. Res.*, *90*, 2085–2090, 1985.

Jacob, D. J., S.-M. Fan, S. C. Wofsy, P. A. Spiro, P. S. Bakwin, J. A. Ritter, E. V. Browell, G. L. Gregory, D. R. Fitzjarrald, and K. E. Moore, Deposition of ozone to tundra, *J. Geophys. Res.*, *97*, 16,473–16,479, 1992.

Johansson, C., Pine forest: A negligible sink for atmospheric NOx in rural Sweden, *Tellus, Ser. B*, *39*, 426–438, 1987.

Johansson, C., and L. Granat, An experimental study of the dry deposition of gaseous nitric acid to snow, *Atmos. Environ.*, *20*, 1165–1170, 1986.

Kasibhatla, P. S., H. Levy II, and W. J. Moxim, Global NOx, HNO3, PAN, and NOy distributions from fossil fuel combustion emissions: A model study, *J. Geophys. Res.*, *98*, 7165–7180, 1993.

Kerstiens, G., and K. J. Lendzian, Interactions between ozone and plant cuticles, *New Phytol.*, *112*, 13–19, 1989.

Kisser-Priesack, G. M., I. Scheunert, and G. Gnatz, Uptake of $^{15}NO_2$ and ^{15}NO by plant cuticles, *Naturwissenschaften*, *74*, 550–551, 1987.

Kramm, G., R. Dlugi, and H. Müller, On the determination of dry deposition fluxes of ozone, nitric oxide and nitric dioxide, *Eurotrac Newsl.*, *11*, 2–9, 1993.

Lee, Y., and S. E. Schwartz, Evaluation of the rate of uptake of nitrogen dioxide by atmospheric and surface liquid water, *J. Geophys. Res.*, *86*, 11971–11983, 1981.

Lenschow, D. H., D. Pearson Jr., and B. Boba Stankov, Measurements of ozone vertical flux to ocean and forest, *J. Geophys. Res.*, *87*, 8833–8837, 1982.

Leuning, R., M. H. Unsworth, H. H. Neumann, and K. M. King, Ozone fluxes to tobacco and soil under field conditions, *Atmos. Environ.*, *13*, 1155–1163, 1979.

Levy, H, II, and W. J. Moxim, Simulated global distribution and deposition of reactive nitrogen emitted by fossil fuel combustion, *Tellus, Ser. B*, *41*, 256–271, 1989.

Lohmann, U., R. Sausen, L. Bengtsson, U. Cubasch, J. Perlwitz, and E. Roeckner, The Köppen climate classification as a diagnostic tool for general circulation models, *Clim. Res.*, *3*, 177–193, 1993.

Massman, W. J., J. Pederson, A. Delany, D. Grantz, G. den Hartog, H. H. Neumann, S. P. Oncley, R. Pearson Jr., and R. H. Shaw, An evaluation of the regional acid deposition model surface module for

ozone uptake at three sites in the San Joaquin Valley of California, *J. Geophys. Res.*, *99*, 8281–8294, 1994.

McKay, W. A., B. A. Stephens, and G. J. Dollard, Laboratory measurements of ozone deposition to sea water and other saline solutions, *Atmos. Environ., Part A*, *26*, 3105–3110, 1992.

Müller, J., Geographical distribution and seasonal variation of surface emissions and deposition velocities of atmospheric trace gases, *J. Geophys. Res.*, *97*, 3787–3804, 1992.

Neubert, A., D. Kley, and J. Wildt, Uptake of NO, NO2 and O3 by sunflower (*Helianthus annuus* L.) and tobacco plants (*Nicotiana tabacum* L.): Dependence on stomatal conductivity, *Atmos. Environ., Part A*, *27*, 2137–2145, 1993.

Olson, J., J. A. Watts, and L. J. Allison, Major world ecosystem complexes ranked by carbon in live vegetation: A database, *Rep. NDP-017*, 164 pp., Oak Ridge Natl. Lab., Oak Ridge, Tenn., 1985.

Padro, J., Seasonal contrasts in modelled and observed dry deposition velocities of O3, SO2 and NO2 over three surfaces, *Atmos. Environ., Part A*, *27*, 807–814, 1993.

Penner, J. E., C. S. Atherton, J. Dignon, S. J. Ghan, and J. J. Walton, Tropospheric nitrogen: A three-dimensional study of sources, distributions and deposition, *J. Geophys. Res.*, *96*, 959–990, 1991.

Ritter, J. A., J. D. Barrick, C. E. Watson, G. W. Sachse, G. L. Gregory, M. A. Woerner, C. E. Watson, G. F. Hill, and J. E. Collins Jr, Airborne flux measurements of trace species in an arctic boundary layer, *J. Geophys Res.*, *97*, 16,601–16,625, 1992.

Ritter, J. A., J. D. Barrick, C. E. Watson, G. W. Sachse, G. L. Gregory, B. E. Anderson, M. A. Woerner, and J. E. Collins Jr, Airborne boundary layer flux measurements of trace gas species over Canadian boreal forest and northern wetland regions, *J. Geophys. Res.*, *99*, 1671–1685, 1994.

Roeckner, E., et al., Simulations of the present-day climate with the ECHAM model: Impact of model physics and resolution, *Rep. 93*, Max-Planck-Institut für Meteorol., Hamburg, Germany, 1992.

Roelofs, G.-J., and J. Lelieveld, Distribution and budget of O_3 in the troposphere calculated with a chemistry-general circulation model, *J. Geophys. Res.*, in press, 1995.

Schwartz, S. E., Factors governing dry deposition of gases to surface water, in *Precipitation Scavenging and Atmosphere-Surface Exchange*, vol. 2, edited by S. E. Schwartz and W. G. N. Slinn, pp. 789–801, Hemisphere, Washington, D. C., 1992.

Sehmel, G. A., Particle and gas dry deposition: A review, *Atmos. Environ.*, *14*, 983–1011, 1980.

Sellers, P. J., Y. Mintz, Y. C. Sud, and A. Dalcher, A simple biosphere model (SiB) for use within general circulation models, *J. Atmos. Sci.*, *43*, 505–531, 1986.

Stocker, D. W., D. H. Stedman, K. F. Zeller, W. J. Massman, and D. G. Fox, Fluxes of nitrogen oxides and ozone measured by Eddy correlation over a shortgrass prairie, *J. Geophys. Res.*, *98*, 12,619–12,630, 1993.

Thoene, B., P. Schröder, H. Papen, A. Egger, and H. Rennenberg, Absorption of atmospheric NO2 by spruce (*Picea abies* L. Karst.) trees, I, NO2 influx and its correlation with nitrate reduction, *New Phytol.*, *117*, 575–585, 1991.

Valdez, M. P., R. C. Bales, D. A. Stanley, and G. A. Dawson, Gaseous deposition to snow, I, Experimental study of SO2 and NO2 deposition, *J. Geophys. Res.*, *92*, 9779–9787, 1987.

Van Pul, W. A. J., The flux of ozone to a maize crop and the underlying soil during a growing season, Ph.D. thesis, Wageningen Agric. Univ., Wageningen, Netherlands, 1992.

Wesely, M. L., D. R. Cook, and R. M. Williams, Field measurements of small ozone fluxes to snow, wet bare soil, and lake water, *Boundary Layer Meteorol.*, *20*, 459–471, 1981.

Wesely, M. L., J. A. Eastman, and E. D. Yalvac, An Eddy correlation measurement of NO2 flux to vegetation and comparison to O3, *Atmos. Environ.*, *16*, 815–820, 1982.

Wesely, M. L., Parameterization of surface resistances to gaseous dry deposition in regional-scale numerical models, *Atmos. Environ.*, *23*, 1293–1304, 1989.

Wilson, M. F., and A. A. Henderson-Sellers, A global archive of land cover and soils data for use in general circulation climate models, *J. Climatol.*, *5*, 119–143, 1985.

L. Ganzeveld and J. Lelieveld, Department of Air Quality, Wageningen University, P.O. Box 8129, 6700 EV, Wageningen, Netherlands. (e-mail: Laurens.Ganzeveld@AirQuality.LUVO.WAU.NL)

(Received January 2, 1995; revised June 14, 1995;
accepted July 6, 1995.)